Volume 25
Number 8
21 April 2025
Pages 1891–2120

Lab on a Chip

Devices and applications at the micro- and nanoscale

rsc.li/loc

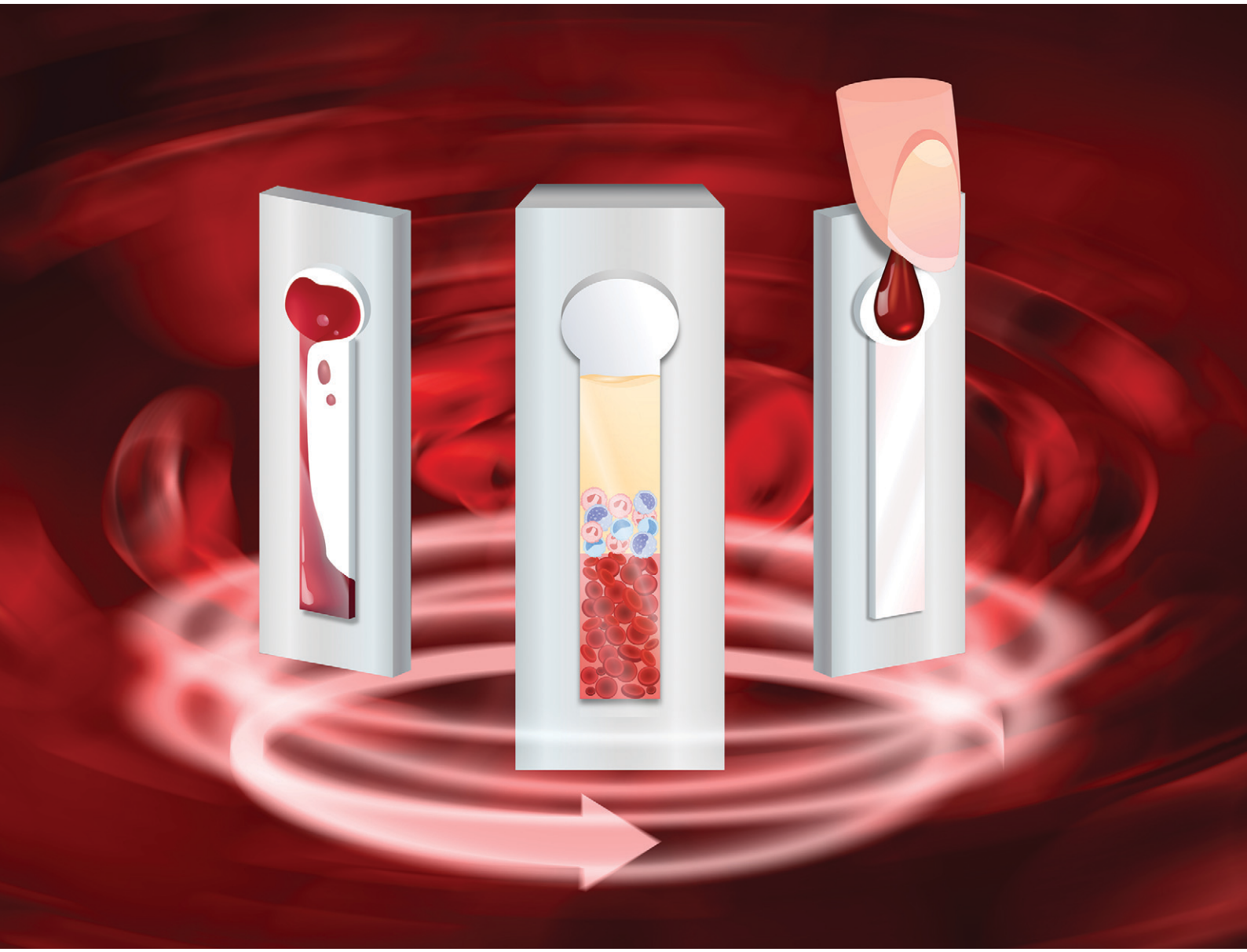

ISSN 1473-0197

ROYAL SOCIETY OF CHEMISTRY

PAPER

H. Cumhur Tekin *et al.*

Dynamic fluidic manipulation in microfluidic chips with dead-end channels through spinning: the Spinochip technology for hematocrit measurement, white blood cell counting and plasma separation

Lab on a Chip

PAPER

View Article Online
View Journal | View Issue

Cite this: *Lab Chip*, 2025, **25**, 1926

Dynamic fluidic manipulation in microfluidic chips with dead-end channels through spinning: the Spinochip technology for hematocrit measurement, white blood cell counting and plasma separation†

Cemre Oksuz,[a] Can Bicmen[b] and H. Cumhur Tekin *[acd]

Centrifugation is crucial for size and density-based sample separation, but low-volume or delicate samples suffer from loss and impurity issues during repeated spins. We introduce the "Spinochip", a novel microfluidic system utilizing centrifugal forces for efficient filling of dead-end microfluidic channels. The Spinochip enables versatile fluid manipulation with a single reservoir for both inlet and outlet functions. It expels compressed air, facilitating fluid flow, and offers programmable filling mechanisms based on the hydraulic resistance of microfluidic channels. Compatible with a basic centrifuge, it allows sequential filling, internal mixing, and collection in straight microfluidic channels by simply adjusting the spinning speed, eliminating the need for complex valving. We demonstrated the Spinochip's efficacy in blood testing, where it successfully separated blood components, such as plasma, buffy coat, and red blood cells, from a single drop using centrifugation alone. This system enabled simultaneous hematocrit (R^2 >0.99) and total white blood cell (R^2 >0.93) quantification within a single microfluidic channel without the need for staining or special reagents. Remarkably, the Spinochip can perform hematocrit measurements on as little as 100 nL of blood, potentially paving the way for less invasive blood analysis. This innovative approach unlocks new possibilities in microfluidics, providing precise fluidic control and centrifugation for sample volumes as small as a few nanoliters.

Received 19th November 2024,
Accepted 13th January 2025

DOI: 10.1039/d4lc00979g

rsc.li/loc

Introduction

Centrifugation is one of the most common and essential methods used for processing of a heterogeneous biological sample, facilitating crucial tasks such as isolation of cells and subgroups, precipitation of nucleic acids, and purification in routine clinical tests and many laboratories.[1,2] It is particularly suitable for isolation of cells by taking advantage of their differences in density, size, and shape.[3,4] However, multiple centrifugation steps lead to important problems such as sample loss, low yield, and purity.[5,6] To overcome these barriers, microfluidic technologies offer a promising solution for sample preparation through centrifugation.[7] However, traditional microfluidics containing inlets and outlets possess potential leakage issues during centrifugation.[8,9] To solve these problems, much attention has been focused on dead-end microfluidics and their controlled fluid handling. For this purpose, the air permeability of the chip material was used to fill the dead-end channels and made it suitable for centrifugation.[10,11] Although prior efforts have explored the utilization of permeability of the chip material to enable filling in dead-end channels, this approach has proven to be impractical due to the lengthy filling times it entails, thus hindering its adaptation.

Centrifugal forces can also be used for fluidic manipulation in microfluidics.[12] Centrifugal microfluidics such as lab-on-a-CD/lab-on-a-disc provide great convenience in microfluidics by providing liquid control that eliminates the use of components such as pumps and actuators.[13] These systems are operated on a motor and enable fluid manipulation operations, including mixing, metering, pumping, and valving.[12–14] Complex assay protocols can also be realized on these centrifugal microfluidic systems using passive and active valve structures. Passive valves including

[a] *Department of Biotechnology and Bioengineering, Izmir Institute of Technology, Izmir 35430, Turkiye*
[b] *Department of Medical Microbiology, Dr. Suat Seren Training and Research Hospital for Chest Diseases and Chest Surgery, Izmir 35430, Turkiye*
[c] *Department of Bioengineering, Izmir Institute of Technology, Izmir 35430, Turkiye. E-mail: cumhurtekin@iyte.edu.tr*
[d] *METU MEMS Center, Ankara 06520, Turkiye*

† Electronic supplementary information (ESI) available. See DOI: https://doi/org/10.1039/d4lc00979g

capillary, siphon, and Coriolis valves do not require any moving part or an external force to regulate flow.[13,15–18] In contrast, active valves, such as pinch, wax and magnetic valves, need either moving internal components or external forces to control flow.[16,19,20] However, centrifugal microfluidic systems require complex system architecture and specialized rotating equipment for automated protocols, thereby limiting their wide adaptation.[12,14,18] Moreover, vent holes on these devices play a crucial role in transferring of samples between chambers by releasing air pressure, although they also pose potential leakage risks.[21,22]

Centrifugal microfluidic devices can also be utilized for blood analysis by separating plasma, serum and cell fractions.[23,24] For instance, a centrifugal microfluidic disc was developed for blood plasma separation.[25] Blood cells were sedimented with the centrifugation and separated from plasma, but sudden acceleration and deceleration can cause disruption of the plasma blood–cell interface. Afterwards, by increasing the rotation speed, the separated plasma was transferred to the collection chamber through a siphon valve. Furthermore, a centrifugal disc platform with curved and branched channels was used for blood plasma separation.[26] As the disc rotates, plasma and blood cells flow towards two different chambers due to the Zweifach–Fung effect. Serum separation through membrane filtration was also realized on a centrifugal disc platform.[27] Additionally, a microfluidic disc was employed to separate white blood cells using a density gradient medium.[28] After centrifugation, white blood cells were layered on top of the density gradient medium with plasma, while red blood cells were sedimented to the bottom. By increasing the rotation speed, separated plasma and white blood cells were transferred into different chambers *via* siphon valves for collection. Moreover, isolation of peripheral blood mononuclear cells was achieved on a centrifugal disc platform using a density gradient medium in a spiral channel.[29] During centrifugation, red blood cells and polymorphonuclear cells moved towards the outer channel wall due to the dominant centrifugal force surpassing the buoyancy force. In contrast, peripheral blood mononuclear cells remained at the interface between the sample and the density gradient medium and were subsequently collected through a different outlet. Furthermore, a centrifugal disc was utilized for differential white blood cell counting by incorporating solution metering and mixing capabilities.[30] Sample preparation was achieved automatically on the platform, followed by hematocrit measurement and differential white blood cell analysis using staining and image processing techniques. For hematocrit measurements, red blood cells were separated from plasma by centrifugation. For white blood cell counting, reagents were initially transferred to the metering chambers and subsequently to the mixing chamber *via* siphon valves through centrifugation. Afterwards, the blood sample was introduced and the mixing of the sample with the reagents occurred by rotating the platform in different directions. Furthermore, a centrifugal disc was used for density gradient and immunoaffinity-based isolation of natural killer cells from whole blood.[31] Ferrowax valves controlled with laser were utilized for transferring separated fractions in different chambers. The density gradient medium was also utilized further in a centrifugal-microfluidic platform to analyze white blood cell subgroups with staining.[32] Similarly, such media have been employed on spinning discs to separate blood components for hematocrit, red blood cell, white blood cell, and platelet analysis through size-based microscopic inspections.[33] Although these centrifugal microfluidic devices have been applied to blood analysis, they often require valves, which complicates device design, fabrication and protocol operation. Additionally, the need for outlet or vent connections poses a potential risk of sample loss due to leakage during spinning. Furthermore, they may require specialized instruments for operation, large sample volumes, sample treatment or staining, additional reagents, or special channel specifications—all of which can limit their usability and hinder widespread adoption.

Here, we present the 'Spinochip', an innovative microfluidic platform that leverages centrifugal forces to achieve efficient filling of dead-end channels. The Spinochip transforms fluid manipulation by utilizing a single reservoir that functions as both the inlet and the outlet, and it uniquely expels compressed air to drive fluid flow. This system features programmable filling mechanisms tailored to the hydraulic resistance of various channels, enabling a wide range of applications. Importantly, the Spinochip operates with a standard centrifuge, facilitating sequential filling, internal mixing, and sample collection without the need for complex valving systems. In blood testing applications, the Spinochip effectively separates plasma, buffy coat, and red blood cells from a minute blood sample, enabling on-chip hematocrit and white blood cell measurements without any staining or reagents. This technology represents a significant advancement in microfluidics, offering precise control and efficient centrifugation for even the smallest sample volumes.

Experimental

Microfluidic chip fabrication

The microfluidic chips were fabricated from 75 μm thick double-sided adhesive (DSA) (Thorlabs, OCA8146-3), 2 mm thick polymethyl methacrylate (PMMA) (Depodanmalzeme, SBB2001) and 1 mm thick glass slides (SinerjiLab, C100000). For this purpose, PMMA and DSA were patterned using a laser cutter (MakeBlock, MLP-K503-40W). Afterwards, the chips were fabricated by bonding PMMA pieces to glass slides using DSA pieces (Fig. S1a†). The DSA thickness (75 μm) gave the channel height value. For different channel heights (75–225 μm), multiple DSA pieces were utilized.

To diminish the channel dimensions, polydimethylsiloxane (PDMS)-based microfluidic chips were utilized. For this purpose, SU-8 molds were fabricated on a silicon (Si) wafer. First, the wafer was cleaned with isopropyl alcohol (IPA) (LuxorKimya) and then dried with N_2 gas. To

coat 30 μm SU-8100 negative photoresist (Microchem), a rotation speed of 1000 rpm was used. Then a soft baking step was applied for 3 min and 7 min at 65 °C and 95 °C, respectively. Afterwards, the SU-8 layer was exposed for 27 s to ultraviolet light with a power of 8 mW cm^{-2}. Subsequently, post exposure baking was conducted for 1 min at 65 °C, followed by 3 min at 95 °C. To reveal the SU-8 structures, SU-8 development was conducted in propylene glycol methyl ether acetate (PGMEA) (Isolab, 484 431) and then the wafer was cleaned with IPA and dried. For PDMS chip fabrication, PDMS (Dow Corning Sylgard 184) prepared with 1 : 10 (w/w) curing agent and base ratio was poured onto the SU-8 molds and kept in an oven (Memmert, UN30) at 65 °C overnight to cure. Then, the PDMS was removed from the mold and a reservoir was opened with a 3 mm diameter punch. After the PDMS and glass slide were treated with air plasma at 100 W, 0.5 mbar for 2 min (Diener Electronic, Zepto LF), they were bonded together to form the chips (Fig. S1b†). After production of PDMS chips, to verify the channel width and height, a channel cross section was analyzed using SEM.

Fabrication and usage of rotating platform

A rotating platform, microfluidic sockets with different angles and apparatus were 3D printed using Ultimaker 2+ (Ultimaker) using polylactic acid (PLA) (Ultimaker, 1609). Microfluidic sockets with different angles (0–90°) were glued to the platform. For filling experiments with minimum rotation speed, the rotating platform with a 45° microfluidic socket was used. The microfluidic chip was placed in a microfluidic socket and the rotating platform was placed onto a spin coater device (Midas, spin process controller). Different channels with varying widths (1–4 mm) and heights (75–225 μm) were subjected to a fixed rotation time of 5 min starting from 100 rpm to the rotation speed where the channel is filled completely. The platform was also tested using microfluidic sockets with different angles (0–90°). For these experiments, channels with dimensions of 3 mm × 25 mm × 0.15 mm ($w \times l \times h$) were rotated for a fixed time of 5 min starting at 400 rpm. For filling profile experiments, a smartphone (Iphone 7, Apple) was placed in the phone socket of the rotating platform to record video (Fig. S2†). Channels with different widths, lengths and fixed heights (0.15 mm) were subjected to constant rpm (500 rpm) to examine the flow profile and the volume inside the channel was analyzed every 0.5 s. Filling rate was calculated as percentage volume divided by second. First, the local maximum filling rate was determined from the peak value and according to this rate, subsequent local peak filling rate intervals were determined for each channel. For sequential filling of microfluidic channels from a single reservoir, food dyes (Deembro, deemk3) were diluted with distilled water at a 1 : 10 (v/v) ratio. Then, red, green, and blue food dyes were prepared in glycerol (Sigma Aldrich, G9012-100ML) at ratios of 1 : 2 (v/v), 1 : 4 (v/v), and 1 : 6 (v/v), respectively. These dyes were introduced into the channels, with dimensions of 3 mm × 25 mm × 0.15 mm ($w \times l \times h$), by rotating the chip one by one at 400 rpm for 1 min. Then, the chip was turned upside down (*i.e.*, the reservoir is oriented on the bottom) and rotated at 400 rpm for 1 min, allowing the liquids to mix in the channel. At this configuration, the mixed liquid can be collected into the reservoir by rotating the chip at 500 rpm for 2 min. For sequential liquid filling from different reservoirs, chips having channels with widths of 4 mm, 2 mm and 1 mm, which were connected to different reservoirs and were merged to a single channel, were used. By holding the chip upside down, food dyes were pipetted inside the closed reservoirs (Fig. S1c†) to eliminate liquid flow between reservoirs. The chip was placed on the platform and exposed to rotation speeds of 350 rpm, 500 rpm and 700 rpm for 30 s. Thus, food dyes with a channel width of 4 mm (red), 2 mm (blue) and 1 mm (green) were filled, respectively.

Fabrication of chip apparatus for centrifuge device and its usage

The apparatus for the centrifuge device was 3D printed using Ultimaker 2+ (Ultimaker) using PLA (Ultimaker, 1609). This apparatus has a diameter of 28 mm and a length of 96 mm suitable for the centrifuge sockets (Fig. S3†). There is a 6 mm opening on it so that the microfluidic chip can be placed in the apparatus and remain stable. For experiments, the chip was placed in the apparatus with its reservoir facing the center of the centrifuge device. Since the rotating platform became unstable after 2000 rpm, the chips were analyzed in a centrifuge device with this apparatus for high rotation speeds. The centrifuge device (Nuve NF 800R) in which the apparatus is placed has a fixed angle of 45° and a rotor radius of 108.4 mm. These features are similar to that of the rotating platform. The filling performance of microfluidic chips having different geometries was evaluated using solutions of different viscosities (1–10 cP) achieved by diluting (0–100%) glycerol with phosphate buffered saline (PBS) (Gibco 10010023), all tested in the centrifuge device with the presented apparatus. In the context of channel geometries with small cross-sectional area achieved in PDMS chips, we conducted experiments introducing 5 μL of blue food color solution in the reservoirs. The filling process was accomplished through centrifugation at 3000 rpm for a duration of 10 min. Subsequently, this apparatus was employed for the measurement of hematocrit and white blood cell levels in blood samples.

Blood analysis

Residual whole blood samples were taken with ethical approval (2022/26-33) from Dr. Suat Seren Chest Diseases and Surgery Training and Research Hospital (Izmir/Turkiye). Informed consent was obtained from all participants for the use of their discarded blood. Dead-end microfluidic channels with dimensions of 3 mm × 25 mm × 0.15 mm ($w \times l \times h$) were used for analyzing blood samples. 10 μL of the whole blood sample taken from an EDTA-coated blood

tube was placed in the reservoir of the chip and then the chip was centrifuged at different centrifugation speeds (1000–4000 rpm) and times (5–15 min). After centrifugation, the number of cells remaining in the plasma and hematocrit were examined with images taken using an inverted microscope (Zeiss Axio Vert A1) and a smartphone (Xiaomi Note 8 Pro), respectively. The hematocrit value was calculated by dividing the total thickness of the red blood cell region by the total thickness of the whole blood region. To create the calibration curve for hematocrit experiments, the blood samples were analyzed in the Spinochip and microhematocrit tube (Isolab, I.088.02.002) at 4000 rpm for 10 min. For on-chip hematocrit measurement in the 2 nL channel fabricated from PDMS, whole blood was introduced into the reservoir and then the sample was filled into the channel by spinning at 3000 rpm for 10 min. Subsequently, centrifugation at 6000 rpm for 5 min was performed to separate the red blood cells from the plasma, enabling the hematocrit measurement. For the 250 nL channel fabricated using PMMA, blood was introduced into the reservoir and separation was performed at 4000 rpm for 10 min. For microhematocrit measurements, after the whole blood sample was filled into the microhematocrit tube, the two ends of the tube were sealed and the tube was placed in the centrifuge device with the microhematocrit apparatus. The microhematocrit apparatus (Fig. S4†) was 3D printed using Ultimaker 2+ (Ultimaker) using PLA (Ultimaker, 1609). This apparatus has dimensions suitable for the sockets of the centrifuge device (28 mm diameter, 96 mm length). There is a 3 mm diameter opening for the microhematocrit tube to remain stable in the apparatus during centrifugation. By placing this apparatus in the centrifuge device, the blood is separated in the tube. The hematocrit values were calculated in the microhematocrit tubes as in the Spinochip from the images taken with a smartphone. To examine the buffy coat region within the dead-end microfluidic channel, 10 μL of blood sample was mixed with Hoescht dye (Invitrogen, H3570) at a ratio of 1 : 1000 (v/v) and incubated for 15 min at 37 °C in the dark. Then, the chip was centrifuged at 4000 rpm for 10 min and the buffy coat region was confirmed under the microscope. White blood cell (WBC) concentration was correlated with the buffy coat thickness. For this purpose, buffy coat thickness measurements were conducted using the ImageJ program from brightfield images. With this program, the thickness of the buffy coat region formed between plasma and red blood cells and containing the WBC population is measured. Measurements were taken in 6 different positions separated equally along the channel and then the average was utilized as a buffy coat thickness. To create a calibration curve for WBC concentration experiments, blood samples diluted in PBS (Gibco, 10010023) were evaluated in the Spinochip by centrifugation at 4000 rpm for 10 min. The same sample was evaluated with a hemocytometer (Isolab 075.03.002, Germany) after staining the sample with Hoescht dye to identify WBCs. The on-chip hematocrit measurements were validated using the microhematocrit method, while the on-chip WBC measurements were confirmed by hemocytometer counting. Hematocrit and WBC concentrations were calculated from the calibration curves and compared with the clinical results obtained with a Coulter counter (Beckman Coulter DxH 900). All the analyses were conducted on fresh blood samples.

To collect blood plasma, a chip containing a reservoir and a collection port was fabricated from PMMA, DSA and glass slides (Fig. S1†). 10 μL whole blood sample was introduced in the reservoir, and the chip was centrifuged at 4000 rpm for 10 min. Afterwards, the plasma region above the buffy coat region was collected from the collection port by pipetting.

Statistical analyses

All experiments were performed in three replicates and quantitative data are shown as mean ± standard deviation (SD). All data were statistically verified using GraphPad Prism v8.0.2 (GraphPad Software Inc., San Diego). The coefficient of determination (R^2 value) was evaluated using linear regression with 95% confidence interval. Clinical data were evaluated using the Bland–Altman % difference method for the mean of three replicates. One-way and two-way ANOVA were performed, and the statistical difference was set at $p < 0.05$.

Results and discussion

Principles of the Spinochip

Experiments conducted for the characterization of the filling principle were performed on a clockwise rotating platform containing a microfluidic socket, where the socket makes a 45° angle (α) with the platform and the distance of the socket from the center is 108.4 mm (r) (Fig. 1a and S2†). The channels were fabricated from PMMA, double-sided adhesive and glass slides using a laser cutter (Fig. S2a†). The forces applied on the Spinochip device, including centrifugal force (F_c), Coriolis force (F_{cor}) and capillary force (F_{cap}), overcome the air pressure in the channel and make the dead-end channel filling as follows (Fig. 1b). Following the placement of the sample in the reservoir, the microfluidic chip was rotated at a predetermined rotation speed, resulting in the application of F_c on the liquid within the reservoir:

$$F_c = \rho\omega^2 r \quad (1)$$

where ρ is the density of the liquid, ω is the rotation speed (rad s^{-1}) and r is the distance of the liquid from the center of a centrifuge device.[33] Moreover, F_{cor} occurs in the opposite direction of the rotation of the disc:

$$F_{cor} = 2\rho\omega U \quad (2)$$

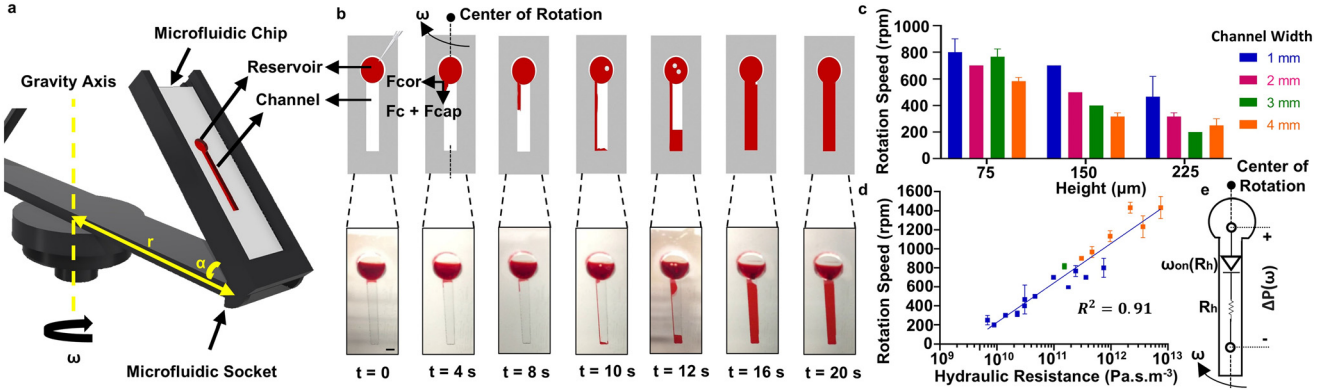

Fig. 1 Principle of the Spinochip technology. (a) Rotating platform mounted on a spin-coater to fill dead-end microfluidic channels. The socket angle α is 45°, the distance of the socket from the rotation center r is 108.4 mm and ω is the rotation speed in the clockwise direction. (b) Illustrations and corresponding photographs of the channel during filling with spinning at 500 rpm. The forces applied in the centrifugal microfluidic channel, F_c, F_{cor} and F_{cap}, create air pressure inside the channel. Air in the channel escapes towards the reservoir (t = 10 s) and the channel is filled with the sample. Scale bar is 3 mm. (c) Required minimum rotation speed for filling channels with 25 mm length but different widths and heights. (d) The relation of the hydraulic resistance of the channels with the required minimum rotational speed for filling. All characterization tests were performed on microfluidic chips fabricated using PMMA. Trials were conducted with different viscosity samples (1–10 cP). Blue, green and orange points represent 1 cP, 5 cP and 10 cP samples, respectively. Error bars are standard deviations from three experiments. 500 rpm rotation speed corresponds to 29.12g force in the platform. (e) The equivalent circuit diagram of a dead-end microfluidic channel with a single reservoir.

with U the average velocity of the liquid. Hence, F_c compels the liquid in the reservoir to penetrate the channel and F_{cor} directs the liquid towards the channel wall, causing it to thin. This increases F_{cap} acting on the liquid:

$$F_{cap} = 2\pi r_c \Upsilon \cos\theta \tag{3}$$

where θ is the contact angle of the fluid, Υ is the surface tension of the liquid and r_c is the radius of the channel.[34] This, in turn, entraps air within the channel, leading to pressurization.

When a liquid enters a microfluidic channel, it also experiences an induced pressure (P_c) that propels it outward from the center of the platform. This pressure is calculated as follows:

$$P_c = \frac{1}{2}\rho\omega^2\left(r_2^2 - r_1^2\right) \tag{4}$$

where r_1 and r_2 are the radial distances from the center of the platform to the liquid's starting and ending points, respectively. Consequently, the induced pressure remains the same in channels of differing dimensions when the liquid is positioned at the same radial distance from the center.

During rotation, the aforementioned forces compress the air within the channel, leading to a steady increase in air pressure. As a result of the pressure difference between the channel and the reservoir, the air eventually escapes toward the reservoir in the form of bubbles. This fundamental process iterates until the channel is completely filled (Video S1†). According to this principle, channel filling occurs when these forces attain sufficient magnitude to overcome channel resistance. We related this mechanism with the hydraulic resistance (R_h) of a standard microfluidic channel having a rectangular cross section:[35]

$$R_h = \frac{1}{1 - 0.63 \times \left(\frac{h}{w}\right)} \times \frac{12\mu l}{h^3 w} \tag{5}$$

where the variables w, l *and* h are the width, length and height of the channel, respectively, and μ is the dynamic viscosity.

It was investigated how the hydraulic resistance, R_h, changes the required minimum rotational speed for filling a dead-end channel on the platform plugged on a spin-coater. For this purpose, the filling in different channels with varying widths and heights was studied for a fixed rotation time of 5 min. It was observed that the required minimum rotational speed for filling decreases with an increase in channel width and height (Fig. 1c). Although the channel can achieve filling within 5 min at a predefined rotational speed (500 rpm) (Fig. 1b and Video S1†), lower rotational speeds (*e.g.*, 350 rpm) combined with prolonged durations (*e.g.*, 60 min) do not result in filling. Furthermore, the hydraulic resistance of the channels show strong correlation with the required rotational speeds for filling (Fig. 1d). Hence, the required rotation speed for filling can be adjusted based on the hydraulic resistance of the channel. Additionally, fluid samples with varying viscosities (1–10 cP) can also be filled successfully into the channel (Fig. 1d). This principle functions as a fluidic diode, where the rotational speed required to initiate flow ($\omega_{on}(R_h)$) is strongly correlated with the channel's hydraulic resistance (Fig. 1e). As a result, these dead-end channels mimic the behavior of a straight channel equipped with a diode at the entrance, activating at a specific rotational speed determined by the channel's hydraulic resistance with an induced pressure (ΔP) on the channel with an applied rotational speed (ω). This mechanism enables

programmable fluidic operations without the need for physical microfluidic valve structures.

Positioning the microfluidic chip at different angles on the platform affects the filling profile because the component of centrifugal force along the channel length changes. To investigate this effect, we examined the chip's filling behavior at a constant rotational speed of 400 rpm, adjusting the angle (α) of the microfluidic socket from 0° to 90° (Fig. S5†). As the angle increases to 60°, the component of centrifugal force acting along the channel becomes insufficient for liquid filling.

In order to understand the limit of the filling principle, we tested it on small microfluidic channel dimensions (down to a channel cross section of 30 μm × 30 μm) that was prepared with PDMS, one of the most used materials for microfluidic fabrication (Fig. S1b†), using a soft-lithography method from SU-8 molds.[36] PMMA and PDMS are hydrophobic materials with surface contact angles greater than 70° and 100°, respectively.[36,37] Although their different surface energies and contact angles lead to different capillary forces, we observed successful filling in both types of channels.[36–39] With the presented strategy, liquid filling was still observed in these channels having a volume of 1.6–5.4 nL (Fig. S6†). The PDMS microfluidic chip was used only to demonstrate filling in the nL channels shown in Fig. S6.† Moreover, not only straight channels can be filled with this strategy; channels with different geometries (such as serpentine and Y-shaped) were also successfully filled (Fig. S7†).

Filling profile in the Spinochip

The flow profile that each channel would show under a constant rotation speed would also be different. Therefore, we investigated the filling volume for different channels as a function of time by applying a constant rotational speed of 500 rpm. As a result, the widest channel shows a faster filling profile, while the filling speed slows down in narrower and longer channels (Fig. 2a). The filling time, defined as the duration required to fill 95% of the total channel volume, exhibits a direct proportionality to the hydraulic resistance of the channels (Fig. 2b). It is noteworthy that this same filling time is achieved even in cases of low hydraulic resistance. To further investigate the filling process, we analyzed the normalized filling rate, which represents the filled volume per unit of time as a percentage of the total volume, in relation to the percentage of filled volume (Fig. 2c). Our findings revealed that the first local maximum filling rate occurred when the volume reached approximately 20.59 ± 4.84% for various channels. This moment corresponds to the bursting of the trapped air, which escapes into the reservoir and results in rapid filling. Prior to this event, according to Boyle's law, the internal pressure within the channel can reach up to 1.037 ± 0.014 atm for a channel with 3 mm width, 0.15 mm height, and 25 mm length (Fig. S8†). Subsequent local peak filling rates were consistently observed at intervals of 26.09 ± 17.42% (calculated by taking peaks bigger than 5% filling rate). Remarkably, at these specific points, we observed air outflow from the channel, coinciding with the inflow of a substantial volume of liquid from the reservoir. At a constant rotational speed (500 rpm), we observed a decrease in average flow rate with increasing channel length for channels of the same cross section (Fig. S9†). This finding indicates that under a constant applied pressure (ΔP), the flow rate is inversely proportional to the hydraulic resistance R_h. Consequently, we modelled each channel as a diode connected in series with its hydraulic resistance (Fig. 1e). Once the induced pressure (ΔP) at angular velocity ω exceeds the diode threshold (ω_{on}) determined by R_h, the channel begins to fill.

Fluidic manipulations in the Spinochip

The presented filling strategy can allow programmable fluidic operation inside dead-end channels. For instance, desired solutions prepared with different glycerol concentrations can be filled sequentially into the dead-end channel from the same reservoir one by one (Fig. 3a). The filled solutions can be mixed inside the channel by flipping the chip upside down in the rotating platform and spinning the chip for 1 min at 400 rpm. At this rotation speed, liquids still remain in the channel. Additionally, the liquid in the dead-end channel can be collected from the reservoir by increasing the

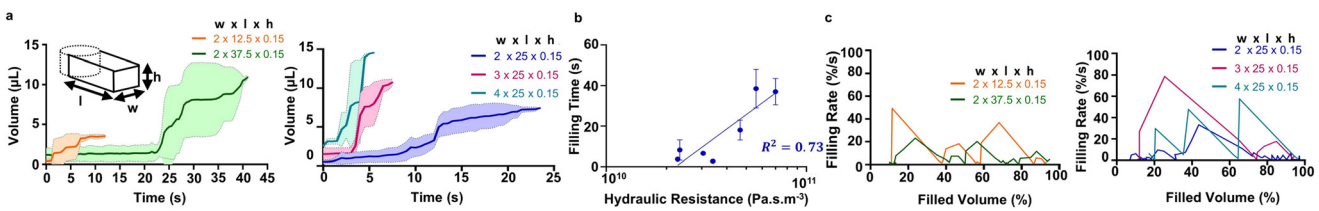

Fig. 2 Flow profiles in the Spinochip devices. (a) Time-dependent volume profile of dead-end channels at 500 rpm. (b) The correlation of the hydraulic resistance of the channels with the filling time of the channels. (c) The filling rate *versus* filled volume of different channels. The data shown in (a) and (c) were obtained by taking the average of three experiments. The data in (b) are presented as means with error bars representing standard deviations of three experiments. *w*, *l* and *h* represent the width, length and height of the channel, respectively, expressed in mm. All characterization tests were performed on microfluidic chips fabricated using PMMA.

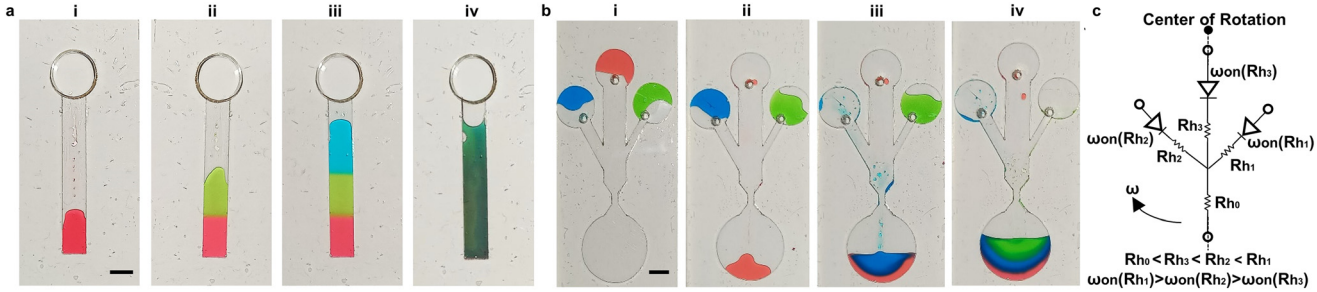

Fig. 3 Programable fluidic operation inside dead-end channels. (a) Solutions filled sequentially from the reservoir one by one (i–iv) at 400 rpm. (b) Sequential filling from different reservoirs. Solutions were added into the reservoirs (i) and the chip was rotated at 350 rpm (ii), 500 rpm (iii) and 700 rpm (iv). The colored solutions in (a) and (b) were prepared in glycerol and distilled water, respectively. Scale bars are 3 mm. (c) The circuit diagram of the chip shown in (b). The hydraulic resistance of the channels with widths of 1, 2, and 4 mm are given as R_{h1}, R_{h2} and R_{h3} and the turn-on rotation speeds of the corresponding fluidic diodes are represented as $\omega_{on}(R_{h1})$, $\omega_{on}(R_{h2})$ and $\omega_{on}(R_{h3})$, respectively. The hydraulic resistance of the main channel is shown as R_{h0}.

spinning rate to 500 rpm (Fig. S10†). Hence, all the solutions can be pipetted out for further operations.

The minimum rotation speed required for channel filling was observed to be dependent on the hydraulic resistance of the channel (Fig. 1d). We applied this principle to enable programmable filling of a dead-end channel from various reservoirs using food dye prepared with distilled water, as depicted in Fig. 3b and Video S2.† Channels of varying widths (*i.e.*, 1, 2, and 4 mm) were connected to separate closed reservoirs (Fig. S1c†), and these channels were interconnected with a primary dead-end channel. By gradually increasing the rotational speed, the solution in the reservoir connected to the wider channel began to flow into the primary channel. This was followed by the solutions from reservoirs connected to narrower channels. This sequential filling occurs due to the differences in hydraulic resistance among the channels and the corresponding rotational speeds required to activate the fluidic diodes in each channel (Fig. 3c). This approach enables precise and programmable manipulation of liquids within dead-end channels, offering potential applications for automated operations.

Blood analysis with the Spinochip

The Spinochip devices with dead-end channels are suitable for precipitation applications through centrifugation, enabling the manipulation of minute samples that are beyond the processing capacity of conventional microcentrifuge tubes. This principle was successfully employed for the separation of blood cells from unprocessed blood samples (10 μL) at high spinning speed (4000 rpm). For this purpose, a blood sample was placed in the reservoir of the microfluidic chip and the chip was introduced into the centrifuge device with a special apparatus (Fig. S3†). After centrifugation of the chip at 4000 rpm for 10 min, three distinct regions, as shown in Fig. 4a, were observed on the chip: plasma (top), buffy coat region (middle) and red blood cells (bottom). When the color of the plasma separated in the channel was compared with the hemolysis reference palette,[40] no hemolysis was observed in the plasma. On the buffy coat region, white blood cells stained with a nuclear dye were clearly observed (Fig. 4b). To effectively precipitate the majority of blood cells, centrifugation at 4000 rpm for 10 min is sufficient (Fig. 4c and S11†). Alternatively, centrifugation at 3000 rpm can be employed for cell precipitation; however, a longer centrifugation duration is required to achieve the same level of plasma purification. Although the red blood cell region remained unaffected across different centrifugation durations at 4000 rpm (Fig. 4d), centrifugation at 4000 rpm (1932*g*) for 10 min was selected as the optimal condition to precipitate nearly all blood cells in specific regions. This on-chip centrifugation at high *g* conditions does not affect cell viability (Fig. S12†). Similarly, the literature reports no damage to blood cells under high *g* forces (*e.g.*, 1500*g*).[41]

We can also collect the separated plasma from the microfluidic chip by using a collection port (Fig. 4e). Since the buffy coat region remains undisturbed during collection, it allows for the preservation of the same purified plasma for off-chip analysis (Fig. 4f). Also, there is no significant difference between the cell number in plasma before and after collection (Fig. 4g).

From the distinct blood regions observed on the Spinochip device, the hematocrit value and white blood cell concentration can be determined by dividing the thickness of the red blood cell region by the thickness of the total blood region and measuring the thickness of the buffy coat region, respectively (Fig. S13†). The on-chip hematocrit and white blood cell measurements conducted in Spinochip devices were calibrated using microhematocrit and hemocytometry analysis, respectively. The results obtained from the on-chip measurements exhibited strong correlations with established gold standard methods, with R^2 values of 0.99 and 0.93 for hematocrit and white blood cell measurements, respectively (Fig. 5a and b). The developed method was tested with 20 clinical patient blood samples and compared with results obtained from the Coulter counter device with the Bland–Altman method (Fig. 5c and d). When comparing the two methods, we observed small mean differences of 5.042% for

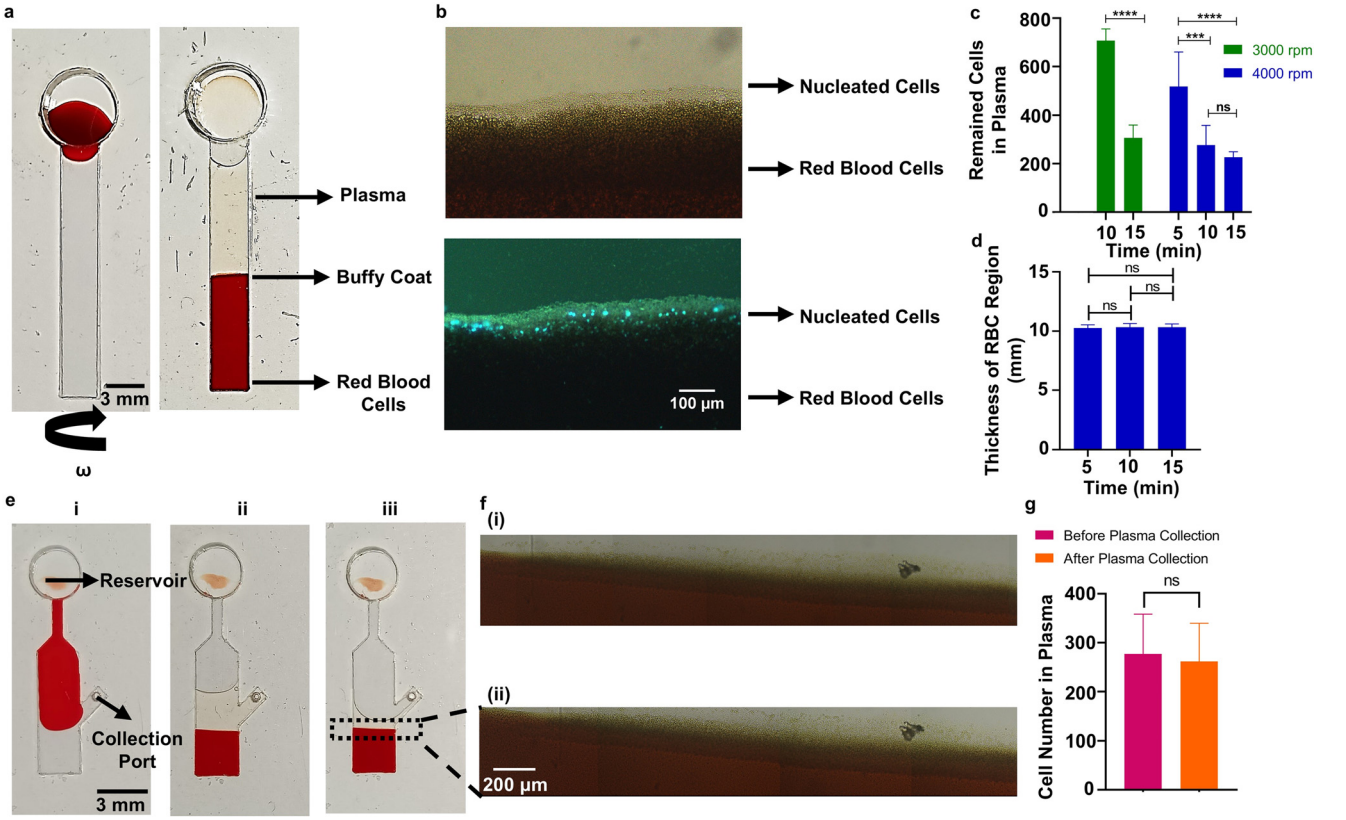

Fig. 4 Separation of blood cells in a Spinochip device. (a) Photographs of the device (i) before and (ii) after centrifugation. (b) Brightfield and fluorescence micrographs of the buffy coat region observed on the device. Blood was stained with Hoescht 33342 for the inspection. (c) Remaining cells in the plasma region of the device for different rotation speeds and durations. d) Thickness of the red blood cell (RBC) region for different rotation durations. (e) Plasma collection steps. (i) First, 10 µL of whole blood is added from a reservoir and (ii) the device is then centrifuged at 4000 rpm for 10 min. (iii) Separated plasma in the device is collected with a pipet from a collection port. The device structure is like in Fig. S1a† and the collection port is in the PMMA layer. (f) A buffy coat region (i) before and (ii) after plasma collection with a pipet from the collection port. (g) Cell number in plasma before and after plasma collection. Data are presented as the mean values with error bars representing the standard deviations from triplicate experiments. A two-way ANOVA with Tukey's multiple comparison test was used for statistical analysis. ns, *** and **** indicate $p > 0.05$, $p \leq 0.001$ and $p \leq 0.0001$, respectively.

hematocrit and 10.4% for white blood cell measurements. Additionally, hematocrit measurements from whole blood samples were achieved using channels with volumes smaller than 2 nL and 250 nL by introducing 100 nL of blood samples into the reservoirs (Fig. 6). The results showed no significant difference between the measurements obtained from the 250 nL channels and standard microhematocrit measurements. However, measurements from the 2 nL channels differed significantly from the microhematocrit values. This discrepancy is attributed to the lack of

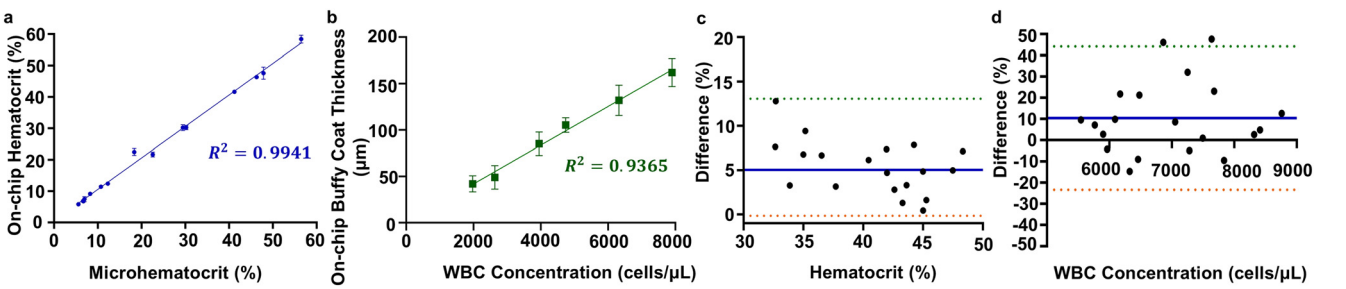

Fig. 5 On-chip hematocrit and white blood cell (WBC) concentration measurements. (a) The calibration curve of hematocrit measurements using the Spinochip and microhematocrit. (b) The calibration curve of buffy coat thickness measured with the Spinochip and actual WBC concentration. Data are presented as the mean values accompanied by error bars representing the standard deviations from triplicate experiments. (c and d) Bland–Altman plots comparing measurements obtained using the Spinochip and the Coulter counter device for hematocrit and WBC concentration, respectively. The solid blue line represents the mean difference and dashed lines represent upper and lower limits (mean ± 1.96 × standard deviation).

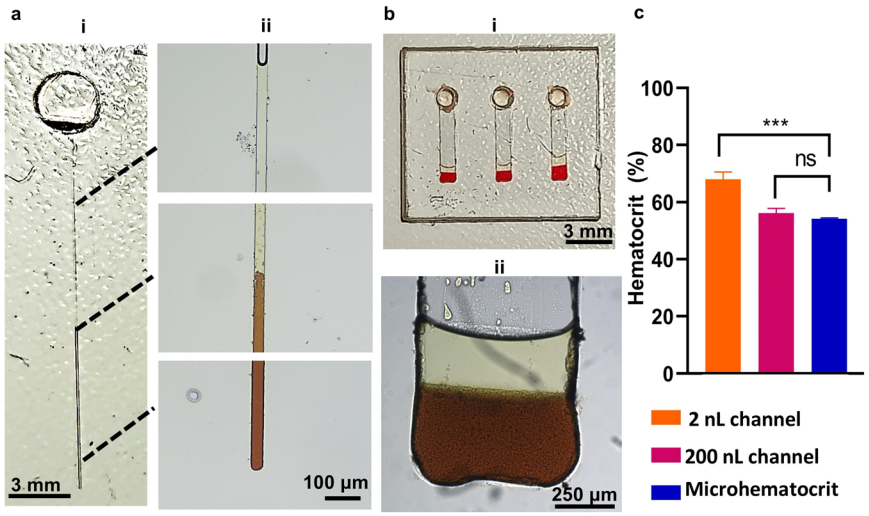

Fig. 6 On-chip hematocrit measurements using 100 nL blood samples. (a) Hematocrit measurement in a 2 nL microfluidic channel. (i) Photograph of the microfluidic chip and (ii) corresponding micrographs showing the separation of red blood cells and plasma within the 2 nL channel. (b) Hematocrit measurement in a 250 nL microfluidic channel. (i) Photograph of the chip featuring three channels and (ii) corresponding micrographs showing blood separation in the 250 nL channel. (c) Comparison of hematocrit measurements obtained from on-chip analysis using 2 nL and 250 nL channels with standard microhematocrit measurements. ns and *** indicate $p > 0.05$ and $p \leq 0.001$, respectively.

equipment capable of accurately pipetting volumes smaller than 2 nL. Consequently, larger volumes were used, leading to a greater amount of sedimented cells and a deviation between the actual results and the observed outcomes.

Comparison of the Spinochip with microfluidic-based blood separation methods

Conventional microfluidic channels typically rely on inlet and outlet ports for operations like centrifugal separation. In these systems, fluid flow is often controlled using a siphon and capillary valves. However, siphon valves require high rotational speeds to fill, leading to uncontrolled drainage and imprecise fluid management.[42–44] Although active valve systems address these issues, they add complexity and cost and require external components.[28,42,45] Alternatively, outlet-free microfluidic chips use material permeability for filling but face challenges such as slow filling times and the need for specific storage conditions.[11,46–48] Our study introduces a novel centrifugal microfluidic platform that overcomes existing limitations by eliminating complex valve structures and reliance on material permeability for filling. Integrating plasma collection, hematocrit measurement, and white blood cell analysis into a single dead-end channel system, it enables efficient, multi-functional blood analysis without external components, reagents, or lengthy workflows. As demonstrated in Table S1,† our technology achieves the highest figure of merit among centrifugal microfluidic devices for blood separation. This figure of merit was calculated by considering various advantages, including the ability to perform the highest number of analyses in the shortest time using the smallest sample volumes, all with the simplest chip design, and its operation without the need for sample treatment, staining, reagents, or additional equipment. Moreover, existing microfluidic systems often focus on tasks like plasma isolation or size-based filtration, with limited capabilities for quantitative analyses such as hematocrit or white blood cell measurements.[49–55] Some microfluidic systems incorporate sample pretreatment, on-chip complex protocols, staining and specialized setups,[49,50,52,54–59] which increase complexity and cost, thereby limiting their usability. As demonstrated in Table S2,† our technology enables multiple analyses on a single chip using minimal, untreated blood samples, offering superior performance compared to other microfluidic systems designed for blood separation.

Conclusion

We introduce the Spinochip technology, which is an innovative method that provides liquid filling into a dead-end channel without using a valve structure by creating air pressure in the channel with rotation and expelling the gas inside the channel as a bubble. This method is a new concept for filling of dead-end channels with programmable fluid operations, enabling sequential filling and collecting of the liquid from the dead-end channel. In addition, the Spinochip technology can separate the whole blood sample in a single channel into three regions as plasma, buffy coat and red blood cells by using only centrifugation. Moreover, for the first time, WBC concentration measurement was achieved from the buffy coat thickness formed in the channel, and the plasma separated in the channel could be collected from the channel with high purity for further analysis. Therefore, our method enables plasma collection, hematocrit measurement, and WBC measurement on the same chip without the need

for staining, sample treatment steps, or additional reagents. It requires minimal blood sample volumes (down to 100 nL) and allows rapid analysis within 10 min. By eliminating the need for valve structures, we have reduced chip complexity and simplified the protocols. The method operates using a simple benchtop centrifuge device without requiring any on-chip venting ports, which ensures robust, leakage-free operation and facilitates seamless integration with existing laboratory workflows. The Spinochip technology enables fluid operation in channels fabricated with different materials at different scales (mm to μm) and various geometries. In the future, thanks to the programmable fluid operation offered, it will allow many fluid manipulations and assays to be performed in an automated manner without using additional elements. It has high potential in point-of-care applications with its advantages of simple fabrication and automated operation. The Spinochip can be applied to various clinical applications that require centrifugation, purification, and enrichment, particularly when dealing with low sample volumes. The Spinochip technology facilitates the straightforward integration of microfluidic technology into various laboratory settings, as it requires only commonly available centrifugal devices found in most laboratories.

Data availability

The data that support the findings of this study are available from the corresponding author upon reasonable request.

Author contributions

Cemre Oksuz: conceptualization, data curation, formal analysis, methodology, validation, data analysis, writing – original draft, visualization; Can Bicmen: providing clinical samples; H. Cumhur Tekin: conceptualization, data curation, formal analysis, methodology, validation, resources, writing – review & editing, supervision, project administration, funding acquisition.

Conflicts of interest

The authors have a patent (2022/015964) associated with the innovation described in this manuscript. H. C. T. is a founder of Saniber Inc., a company dedicated to the development of telemedicine solutions, as well as integrated microfluidic and biomedical devices for point-of-care diagnosis and monitoring. H. C. T.'s interests were diligently reviewed and overseen in strict adherence to the conflict-of-interest policies by IZTECH.

Acknowledgements

The authors acknowledge financial support from The Scientific and Technological Research Council of Turkiye (22AG032) and from Izmir Institute of Technology (IZTECH) (2022-IYTE-2-0056). The authors would like to thank Engin Ozcivici, Ph.D. from the Department of Bioengineering, Izmir Institute of Technology (IZTECH), Turkiye for useful discussion on data interpretation. The Research and Application Center for Quantum Technologies (KUANTAM) at IZTECH, and Dr. Lutfi Ozyuzer from the Department of Physics at IZTECH are acknowledged for providing the cleanroom facilities for microfabrication processes. The authors would like to thank METU MEMS Center, Turkiye for its support for mask fabrication and IZTECH Integrated Research Center (TAM) for SEM analysis. The authors would like to thank Oyku Doyran from the Laboratory of Biomedical Micro and Nanosystems (LBMS), IZTECH for photolithography process, and Sadik Koc and interns (Tugce Haskavuk and Nisa Yeniceri) from LBMS for their assistance during the microfluidic device fabrication. The authors would like to dedicate this article to the loving memories of those lost in the 2023 Kahramanmaras Earthquake.

References

1 Y. Wang, B. B. Nunna, N. Talukder, E. E. Etienne and E. S. Lee, Blood plasma self-separation technologies during the self-driven flow in microfluidic platforms, *Bioengineering*, 2021, **8**(7), 94.
2 V. VanDelinder and A. Groisman, Separation of plasma from whole human blood in a continuous cross-flow in a molded microfluidic device, *Anal. Chem.*, 2006, **78**(11), 3765–3771.
3 W. S. Hu, *Engineering principles in biotechnology*, John Wiley & Sons, 2017.
4 B. Alberts, A. Johnson, J. Lewis, M. Raff, K. Roberts and P. Walter, Fractionation of cells, in *Molecular Biology of the Cell*, Garland Science, 4th edn, 2002.
5 A. Nigro, A. Finardi, M. M. Ferraro, D. E. Manno, A. Quattrini and R. Furlan, *et al.*, Selective loss of microvesicles is a major issue of the differential centrifugation isolation protocols, *Sci. Rep.*, 2021, **11**(1), 3589.
6 A. S. Pina, C. R. Lowe and A. C. A. Roque, Challenges and opportunities in the purification of recombinant tagged proteins, *Biotechnol. Adv.*, 2014, **32**(2), 366–381.
7 G. A. Slusher, P. A. Kottke, A. L. Culberson, M. A. Chilmonczyk and A. G. Fedorov, Microfluidics enabled multi-omics triple-shot mass spectrometry for cell-based therapies, *Biomicrofluidics*, 2024, **18**(1), 011302.
8 O. Strohmeier, M. Keller, F. Schwemmer, S. Zehnle, D. Mark and F. Von Stetten, *et al.*, Centrifugal microfluidic platforms: advanced unit operations and applications, *Chem. Soc. Rev.*, 2015, **44**(17), 6187–6229.
9 K. C. O'Connell and J. P. Landers, Integrated membranes within centrifugal microfluidic devices: A review, *Lab Chip*, 2023, **23**, 3130–3159.
10 A. Wang, S. M. Boroujeni, P. J. Schneider, L. B. Christie, K. A. Mancuso and S. T. Andreadis, *et al.*, An Integrated Centrifugal Degassed PDMS-Based Microfluidic Device for Serial Dilution, *Micromachines*, 2021, **12**(5), 482.
11 C. Oksuz and H. C. Tekin, A Vacuum-Integrated Centrifugal Microfluidic Chip for Density-Based Separation of Microparticles, in *2021 IEEE 34th International Conference on Micro Electro Mechanical Systems (MEMS)*, IEEE, 2021, pp. 1009–1011.

12 R. Gorkin, J. Park, J. Siegrist, M. Amasia, B. S. Lee and J. M. Park, *et al.*, Centrifugal microfluidics for biomedical applications, *Lab Chip*, 2010, 1758–1773.
13 S. Hugo, K. Land, M. Madou and H. Kido, A centrifugal microfluidic platform for point-of-care diagnostic applications, *S. Afr. J. Sci.*, 2014, **110**(1–2), 1–7.
14 R. Gorkin, L. Clime, M. Madou and H. Kido, Pneumatic pumping in centrifugal microfluidic platforms, *Microfluid. Nanofluid.*, 2010, **9**(2–3), 541–549.
15 J. F. Hess, S. Zehnle, P. Juelg, T. Hutzenlaub, R. Zengerle and N. Paust, Review on pneumatic operations in centrifugal microfluidics, *Lab Chip*, 2019, **19**(22), 3745–3770.
16 J. Kim, H. Kido, R. H. Rangel and M. J. Madou, Passive flow switching valves on a centrifugal microfluidic platform, *Sens. Actuators, B*, 2008, **128**(2), 613–621.
17 A. Kazemzadeh, P. Ganesan, F. Ibrahim, M. M. Aeinehvand, L. Kulinsky and M. J. Madou, Gating valve on spinning microfluidic platforms: A flow switch/control concept, *Sens. Actuators, B*, 2014, **204**, 149–158.
18 M. Tang, G. Wang, S. K. Kong and H. P. Ho, A review of biomedical centrifugal microfluidic platforms, *Micromachines*, 2016, **7**(2), 26.
19 S. Peshin, D. George, R. Shiri, L. Kulinsky and M. Madou, Capillary Flow-Driven and Magnetically Actuated Multi-Use Wax Valves for Controlled Sealing and Releasing of Fluids on Centrifugal Microfluidic Platforms, *Micromachines*, 2022, **13**(2), 303.
20 S. Peshin, M. Madou and L. Kulinsky, Microvalves for applications in centrifugal microfluidics, *Sensors*, 2022, **22**(22), 8955.
21 X. Cao, A. J. deMello and K. S. Elvira, Enhanced versatility of fluid control in centrifugal microfluidic platforms using two degrees of freedom, *Lab Chip*, 2016, **16**(7), 1197–1205.
22 T. H. G. Thio, F. Ibrahim, W. Al-Faqheri, N. Soin, M. Kahar Bador and M. Madou, Sequential push-pull pumping mechanism for washing and evacuation of an immunoassay reaction chamber on a microfluidic CD platform, *PLoS One*, 2015, **10**(4), e0121836.
23 X. Chen, C. C. Liu and H. Li, Microfluidic chip for blood cell separation and collection based on crossflow filtration, *Sens. Actuators, B*, 2008, **130**(1), 216–221.
24 M. Iqbal, A. Mukhamedshin, D. L. Lezzar, K. Abhishek, A. L. McLennan and F. W. Lam, *et al.*, Recent advances in microfluidic cell separation to enable centrifugation-free, low extracorporeal volume leukapheresis in pediatric patients, *J. Geophys. Res. Space Physics*, 2023, **21**(6), 494.
25 M. Amasia and M. Madou, Large-volume centrifugal microfluidic device for blood plasma separation, *Bioanalysis*, 2010, **2**(10), 1701–1710.
26 J. N. Kuo and X. F. Chen, Plasma separation and preparation on centrifugal microfluidic disk for blood assays, *Microsyst. Technol.*, 2015, **21**, 2485–2494.
27 K. D. Lenz, S. Jakhar, J. W. Chen, A. S. Anderson, D. C. Purcell and M. O. Ishak, *et al.*, A centrifugal microfluidic cross-flow filtration platform to separate serum from whole blood for the detection of amphiphilic biomarkers, *Sci. Rep.*, 2021, **11**(1), 5287.
28 D. J. Kinahan, S. M. Kearney, N. A. Kilcawley, P. L. Early, M. T. Glynn and J. Ducree, Density-gradient mediated band extraction of leukocytes from whole blood using centrifugo-pneumatic siphon valving on centrifugal microfluidic discs, *PLoS One*, 2016, **11**(5), e0155545.
29 Y. Sun and P. Sethu, Low-stress microfluidic density-gradient centrifugation for blood cell sorting, *Biomed. Microdevices*, 2018, **20**, 1–10.
30 R. Khodadadi, M. Eghbal, H. Ofoghi, A. Balaei, A. Tamayol and K. Abrinia, *et al.*, An integrated centrifugal microfluidic strategy for point-of-care complete blood counting, *Biosens. Bioelectron.*, 2024, **245**, 115789.
31 S. Yang, S. H. Kim, A. Intisar, H. Y. Shin, H. G. Kang and M. Y. Kim, *et al.*, Fully Automated Continuous Centrifugal Microfluidics Isolates Natural Killer Cells with High Performance and Minimal Stress, *Anal. Chem.*, 2023, **95**(26), 9949–9958.
32 S. T. Moen, C. L. Hatcher and A. K. Singh, A centrifugal microfluidic platform that separates whole blood samples into multiple removable fractions due to several discrete but continuous density gradient sections, *PLoS One*, 2016, **11**(4), e0153137.
33 R. Agarwal, A. Sarkar, A. Bhowmik, D. Mukherjee and S. Chakraborty, A portable spinning disc for complete blood count (CBC), *Biosens. Bioelectron.*, 2020, **150**, 111935.
34 W. Al-Faqheri, T. H. G. Thio, M. A. Qasaimeh, A. Dietzel, M. Madou and A. Al-Halhouli, Particle/cell separation on microfluidic platforms based on centrifugation effect: A review, *Microfluid. Nanofluid.*, 2017, **21**(6), 1–23.
35 S. Choi, M. G. Lee and J. K. Parka, Microfluidic parallel circuit for measurement of hydraulic resistance, *Biomicrofluidics*, 2010, **4**(3), 034110.
36 Y. Ma, X. Cao, X. Feng, Y. Ma and H. Zou, Fabrication of super-hydrophobic film from PMMA with intrinsic water contact angle below 90°, *Polymer*, 2007, **48**(26), 7455–7460.
37 J. Wang, Y. Wang, G. Zhang, B. Xu, Z. Zhao and T. Yin, Fabrication of Polymethyl Methacrylate (PMMA) Hydrophilic Surfaces Using Combined Offset-Tool-Servo Flycutting and Hot Embossing Methods, *Polymers*, 2023, **15**(23), 4532.
38 A. Sikora, D. Czylkowski, B. Hrycak, M. Moczała-Dusanowska, M. Łapiński and M. Dors, *et al.*, Surface modification of PMMA polymer and its composites with PC61BM fullerene derivative using an atmospheric pressure microwave argon plasma sheet, *Sci. Rep.*, 2021, **11**(1), 9270.
39 Y. A. Alzahid, P. Mostaghimi, A. Gerami, A. Singh, K. Privat and T. Amirian, *et al.*, Functionalisation of Polydimethylsiloxane (PDMS)- Microfluidic Devices coated with Rock Minerals, *Sci. Rep.*, 2018, **8**(1), 15518.
40 U.S. Centers for Disease Control and Prevention, *Hemolysis Reference Palette*, Available at: **https://www.cdc.gov/vector-borne-diseases/media/pdfs/Hemolysis_Palette_Reference_Tool-P.pdf**, 2025, (Accessed: January 2025).
41 F. Kiss, E. Toth, K. Miszti-Blasius and N. Nemeth, The effect of centrifugation at various g force levels on rheological properties of rat, dog, pig and human red blood cells, *Clin. Hemorheol. Microcirc.*, 2016, **62**(3), 215–227.

42 A. Al-Halhouli, F. B. El, A. Albagdady and W. Al-Faqheri, Development of active centrifugal pump for microfluidic CD platforms, *Micromachines*, 2020, **11**(2), 140.
43 Y. Zhu, Y. Chen and Y. Xu, Interruptible siphon valving for centrifugal microfluidic platforms, *Sens. Actuators, B*, 2018, **276**, 313–321.
44 T. Ju, Working principle and applications of active and passive microfluidic valves, *J. Phys.: Conf. Ser.*, 2022, 012013.
45 L. Clime, J. Daoud, D. Brassard, L. Malic, M. Geissler and T. Veres, Active pumping and control of flows in centrifugal microfluidics, *Microfluidics and Nanofluidics*, Springer Verlag, vol. 23, 2019.
46 G. Firpo, E. Angeli, L. Repetto and U. Valbusa, Permeability thickness dependence of polydimethylsiloxane (PDMS) membranes, *J. Membr. Sci.*, 2015, **481**, 1–8.
47 Y. Yuan, Y. Yalikun, N. Ota and Y. Tanaka, Property investigation of replaceable PDMS membrane as an actuator in microfluidic device, *Actuators*, 2018, 68.
48 L. Xu, H. Lee, D. Jetta and K. W. Oh, Vacuum-driven power-free microfluidics utilizing the gas solubility or permeability of polydimethylsiloxane (PDMS), *Lab Chip*, 2015, **15**(20), 3962–3979.
49 S. B. Berry, S. C. Fernandes, A. Rajaratnam, N. S. DeChiara and C. R. Mace, Measurement of the hematocrit using paper-based microfluidic devices, *Lab Chip*, 2016, **16**(19), 3689–3694.
50 Y. Wang, B. B. Nunna, N. Talukder and E. S. Lee, Microfluidic-Based Novel Optical Quantification of Red Blood Cell Concentration in Blood Flow, *Bioengineering*, 2022, **9**(6), 247.
51 M. V. Bills, B. T. Nguyen and J. Y. Yoon, Simplified White Blood Cell Differential: An Inexpensive, Smartphone- and Paper-Based Blood Cell Count, *IEEE Sens. J.*, 2019, **19**(18), 7822–7828.
52 Y. Zhang, J. Bai, H. Wu and J. Y. Ying, Trapping cells in paper for white blood cell count, *Biosens. Bioelectron.*, 2015, **69**, 121–127.
53 X. Wang, G. Lin, G. Cui, X. Zhou and G. L. Liu, White blood cell counting on smartphone paper electrochemical sensor, *Biosens. Bioelectron.*, 2017, **90**, 549–557.
54 L. P. Murray and C. R. Mace, A Novel Paper-Based Cytometer for the Detection and Enumeration of White Blood Cells According to their Immunophenotype, *Anal. Chem.*, 2022, **29**, 10443–10450.
55 M. Al-Tamimi, M. El-Sallaq, S. Altarawneh, A. Qaqish and M. Ayoub, Development of Novel Paper-Based Assay for Direct Serum Separation, *ACS Omega*, 2023, **8**(23), 20370–20378.
56 U. Hassan, B. Reddy, G. Damhorst, O. Sonoiki, T. Ghonge and C. Yang, *et al.*, A microfluidic biochip for complete blood cell counts at the point-of-care, *Technology*, 2015, **03**(04), 201–213.
57 T. Peng, X. Su, X. Cheng, Z. Wei, X. Su and Q. Li, A microfluidic cytometer for white blood cell analysis, *Cytometry, Part A*, 2021, **99**(11), 1107–1113.
58 A. Mehran, P. Rostami, M. S. Saidi, B. Firoozabadi and N. Kashaninejad, High-throughput, label-free isolation of white blood cells from whole blood using parallel spiral microchannels with u-shaped cross-section, *Biosensors*, 2021, **11**(11), 406.
59 S. Zhu, D. Wu, Y. Han, C. Wang, N. Xiang and Z. Ni, Inertial microfluidic cube for automatic and fast extraction of white blood cells from whole blood, *Lab Chip*, 2020, **20**(2), 244–252.